Geophysical Prospecting, 2008, **56**, 737–749 doi:10.1111/j.1365-2478.2008.00695.x

Two-dimensional joint inversion of radiomagnetotelluric and direct current resistivity data

M. Emin Candansayar[1]* and Bülent Tezkan[2]

[1]*Ankara University, Faculty of Engineering, Department of Geophysical Engineering, 06100, Ankara, Turkey, and* [2]*University of Cologne, Institute of Geophysics and Meteorology, Cologne, Germany*

Received July 2007, revision accepted December 2007

ABSTRACT

An algorithm for the two-dimensional (2D) joint inversion of radiomagnetotelluric and direct current resistivity data was developed. This algorithm can be used for the 2D inversion of apparent resistivity data sets collected by multi-electrode direct current resistivity systems for various classical electrode arrays (Wenner, Schlumberger, dipole-diplole, pole-dipole) and radiomagnetotelluric measurements jointly. We use a finite difference technique to solve the Helmoltz and Poisson equations for radiomagnetotelluric and direct current resistivity methods respectively. A regularized inversion with a smoothness constrained stabilizer was employed to invert both data sets. The radiomagnetotelluric method is not particularly sensitive when attempting to resolve near-surface resistivity blocks because it uses a limited range of frequencies. On the other hand, the direct current resistivity method can resolve these near-surface blocks with relatively greater accuracy. Initially, individual and joint inversions of synthetic radiomagnetotelluric and direct current resistivity data were compared and we demonstrated that the joint inversion result based on this synthetic data simulates the real model more accurately than the inversion results of each individual method. The developed 2D joint inversion algorithm was also applied on a field data set observed across an active fault located close to the city of Kerpen in Germany. The location and depth of this fault were successfully determined by the 2D joint inversion of the radiomagnetotelluric and direct current resistivity data. This inversion result from the field data further validated the synthetic data inversion results.

INTRODUCTION

Electric and electromagnetic (EM) geophysical surveying methods are sensitive to subsurface electrical resistivity structures. Generally, electric and EM data are collected for various purposes and are interpreted using inversion algorithms. However, these inversions are typically non-linear, ill-posed and non-unique. Therefore, the interpretation of inverted electric and EM data always involves certain ambiguities. To mitigate this problem, combined methods are used and more reliable models are obtained by jointly inverting electric and EM data sets. There have been many studies published regarding the joint inversions of different electric and EM methods. This was first shown by Vozoff and Jupp (1975), who introduced the joint inversion algorithm of magnetotelluric and direct current resistivity data. Meju (1996) and Raiche *et al.* (1985) used a 1D joint inversion of transient electromagnetic (TEM) and Schlumberger soundings and TEM and MT soundings, respectively. A 2D joint inversion of MT and dipole-dipole data sets was published by Sasaki (1989). Harinarayana (1999) provided an overview of these efforts by thoroughly reviewing the combined inversion of electric and EM measurements. In recent years the joint inversion of data sets that are sensitive to different physical parameters, e.g., seismic velocity and resistivity, has become increasingly popular. Joint inversion can improve the resolution of subtle features, reduce the influence of noise and limit the range of acceptable models.

*E-mail: candansa@eng.ankara.edu.tr

There are numerous successful 2D inversions of radiomagnetotelluric and direct current resistivity data sets in the literature (Tezkan, Hördt and Gobashy 2000; Özürlan, Candansayar and Şahin 2006), however, a 2D joint inversion combining radiomagnetotelluric and direct current resistivity data has not yet been published. Both of these methods are sensitive to the resistivity properties of underground structures. The radiomagnetotelluric method is an extension of the well-known very-low-frequency technique to higher frequencies (Tezkan 1999) and it uses radio transmitters in a frequency range between 10 kHz and 1 MHz. This method has been used with increasing popularity for different hydrogeological applications (Pedersen, Bastani and Dynesius 2005), environmental applications (Tezkan *et al.* 1996) and structural investigations (Linde and Pedersen 2004).

On the other hand, the direct current resistivity method is the most popular electrical method that has also been used for the same purposes (e.g., Auken *et al.* 2006; Özürlan *et al.* 2006). Direct current resistivity sounding-profiling data are mainly collected by using a multi-electrode system.

The main difference between the joint inversion of MT with direct current resistivity and the joint inversion of radiomagnetotelluric with direct current resistivity is the skin depth differences between MT and radiomagnetotelluric methods. The skin depth is dependent on the resistivity of underground structures and the frequency range used for both methods. Using the MT method, data are generally collected in the 300–0.0001 Hz frequency range, whereas data are measured in the 10 kHz to 1 MHz range for the radiomagnetotelluric method. Therefore, as an example, the skin depth range for MT will be approximately 290–50 300 metres and for radiomagnetotelluric measurement it will be approximately 5–50 metres for a 100 Ωm homogenous half-space. On the other hand, for the direct current resistivity method, the depth of investigation is mainly dependent on the underground resistivity structure and the distance between the electrodes.

It is neither practical nor easy to obtain information using the direct current resistivity method for the depths at which the MT method can operate. Therefore, typically, there will be a gap between the MT and direct current resistivity data when they are interpreted by joint inversion. The direct current resistivity data mainly resolve near-surface structures while MT data resolve deep structures. In the case of a joint inversion of radiomagnetotelluric and direct current resistivity data, there will be almost no gap between these methods and the resolving advantages of both methods are combined to achieve more reliable information about the overall resistivity structure.

In this study, we developed an algorithm for the 2D joint inversion of radiomagnetotelluric and direct current resistivity data. We tested the algorithm using various synthetic data calculated for different models representing different geological settings. The synthetic data inversions showed that the joint inversion of radiomagnetotelluric and direct current resistivity data gives more prominent results than any individual inversion of the data set. In this paper we present one synthetic data inversion result calculated for a model simulating a near-surface fault structure with the same settings also used in the field survey. The field data were collected along two parallel lines, with 115-metre intervals, which crossed an expected fault in Kerpen, approximately 20 km west of Cologne, Germany. The 2D joint inversion results located the fault more accurately than the individual inversions of radiomagnetotelluric and direct current resistivity data.

THE INVERSION ALGORITM

A new inversion algorithm was developed in order to invert the radiomagnetotelluric and direct current resistivity data jointly. It is well known that the inverse problem associated with electric and electromagnetic data is non-linear and ill-posed. Therefore, it has generally been solved by using a regularization method. Here, we used a smoothness-constrained least-squares approach (Tikhonov *et al.* 1995). In this method, the minimization of the objective function yields the normal equations:

$$\left(\mathbf{A}^{\mathrm{T}}\mathbf{W}_{\mathrm{d}}^{\mathrm{T}}\mathbf{W}_{\mathrm{d}}\mathbf{A}+\alpha\mathbf{C}^{\mathrm{T}}\mathbf{C}\right)\Delta\mathbf{m}=\mathbf{A}^{\mathrm{T}}\mathbf{W}_{\mathrm{d}}^{\mathrm{T}}\mathbf{W}_{\mathrm{d}}\Delta\mathbf{d}-\alpha\mathbf{C}^{\mathrm{T}}\mathbf{C}\mathbf{m}^{(\mathrm{k})} \quad (1)$$

where $\mathbf{A}$ is the sensitivity (Jacobian) matrix, $\mathbf{m}^{(k)}$ is the model parameter vector at the k^{th} iteration that comprises the logarithm of unknown block resistivities, $\Delta\mathbf{d}$ is the vector of differences between the modelled response and the observed data, $\Delta\mathbf{m}$ is the parameter correction vector to $\mathbf{m}^{(k)}$, $\mathbf{C}$ is a second–difference operator used to define the model roughness, $\mathbf{W}_d$ is the data weighting matrix having the reciprocal of the data amplitude where data are assumed to have the same percentage standard deviation in diagonal elements and zeros otherwise and α is a regularization parameter. Note that, the logarithm of the observed and the calculated apparent resistivity (for direct current resistivity and radiomagnetotelluric data) and phase of impedance in radians versus frequencies (for radiomagnetotelluric data) are used in inversion and the sensitivity matrix is modified according to these values. The solution of equation (1) for $\Delta\mathbf{m}$ is equivalent to the least-squares solution

of the rectangular system (Haber and Oldenburg 2000):

$$\tilde{\mathbf{A}}\Delta\mathbf{m} = \Delta\tilde{\mathbf{d}} \tag{2}$$

where

$$\tilde{\mathbf{A}} = \begin{bmatrix} \mathbf{W}_d\mathbf{A} \\ \sqrt{\alpha}\mathbf{C} \end{bmatrix} \text{ and } \quad \Delta\tilde{\mathbf{d}} = \begin{bmatrix} \mathbf{W}_d\Delta\mathbf{d} \\ -\sqrt{\alpha}\mathbf{C}\mathbf{m}^{(k)} \end{bmatrix}.$$

In the newly developed algorithm, equation (2) was solved using a QR factorization that produces a result more quickly than the singular value decomposition solution. However, it is known that the singular value decomposition solution is more stable than QR factorization. For this case, the joint inversion of direct current resistivity with radiomagnetotelluric data, $\mathbf{A}$ and $\Delta\mathbf{d}$ were given as below:

$$\mathbf{A} = \begin{bmatrix} \mathbf{W}_{DCR}\mathbf{A}_{DCR} \\ \mathbf{W}_{RMT}\mathbf{A}_{RMT} \end{bmatrix} \text{ and } \quad \Delta\mathbf{d} = \begin{bmatrix} \Delta\mathbf{d}_{DCR} \\ \Delta\mathbf{d}_{RMT} \end{bmatrix} \tag{3}$$

where $\mathbf{A}_{DCR}$, $\mathbf{W}_{DCR}$ and $\mathbf{A}_{RMT}$ and $\mathbf{W}_{RMT}$ were the sensitivity and diagonal weighting matrices for the direct current resistivity and the radiomagnetotelluric methods, respectively. All non-diagonal elements of these two matrices, $\mathbf{W}_{DCR}$ and $\mathbf{W}_{RMT}$, are zero and the diagonal elements of them were equal to one. However, if we wanted to decrease the effect of some data on a given parameter, we changed the related diagonal element of the matrix to a value between 0 and 1.

Assuming the local electromagnetic fields form a plane wave (McNeill and Labson 1991) and neglecting the displacement currents for normal resistivity distributions beneath the survey area (e.g., $\rho < 500$ Ωm), magnetotelluric inversion algorithms can be used for radiomagnetotelluric data interpretation (Candansayar and Tezkan 2006). In our joint inversion algorithm, the finite-difference forward solution and partial derivative matrix calculations (e.g., McGillivray *et al.* 1994) for the MT data inversion were solved using the R2DMTINV algorithm (Candansayar 2008). On the other hand, for the direct current resistivity method the Poisson equation was solved by using the finite difference method (e.g., Dey and Morrison 1978) and the partial derivative matrix was calculated according to Smith and Vozoff (1984) and Tripp, Hohmann and Swift (1984). In our new algorithm the forward solution for the direct current resistivity data can be calculated for all possible classical configurations such as Wenner, Schlumberger, dipole-dipole, left- and right-side pole-dipole. It is also possible to invert the combination of these data sets with the algorithms developed by Candansayar (2006). Candansayar and Başokur (2001) showed that a joint inversion of left- and right-side pole-dipole configurations (AMN and MNB) is superior to any classical four-electrode configuration data inversion. We also used these two electrode configurations in our applications.

To check the evolution of the misfit at every iterative step the RMS (root mean squares) values of normalized residuals of the fitted data were calculated (e.g., Gallardo and Meju 2004)

$$RMS = \sqrt{\frac{(\mathbf{W}_d\Delta\mathbf{d})^T(\mathbf{W}_d\Delta\mathbf{d})}{N}} \tag{4}$$

where N is the number of data. The iteration stops in all inversions when equation (4) can no longer be reduced. Note that, a RMS lower than 1 indicates that the noise has been modelled as well. Therefore, we did not allow the RMS value to be reduced to below 1 in our algorithm.

INVERSION OF SYNTHETIC DATA

We first tested our inversion algorithm using synthetic data. The synthetic data were constructed for a fault model (Fig. 1a) that was similar to the expected structure derived from the inversion of the field data shown in the next section. The model consisted of a resistive surface layer with 100 Ωm resistivity and a 1000 Ωm resistive basement. The first layer represented low resistive loess and the basement layer represented highly resistive gravel. The thickness of the surface layer varied from 13.75 metres at the beginning of the profile and after the middle of the profile its depth reached 18.75 metres. There were also two resistive bodies with a resistivity of 600 Ωm beneath the surface. The first body was situated between −37.5 and −12.5 metres along the line direction and its thickness was 8.75 metres. The second body was situated between 37.5 and 40 metres along the line direction and its thickness was 3.75 metres. The fault was represented by a 150 Ωm conductive fault gauge buried in the resistive gravel. The width of this fault gauge varied between 12.5 and 17.5 metres.

The synthetic data were constructed using a model mesh divided into 100 x 30 blocks (Fig. 1a). The synthetic direct current resistivity and radiomagnetotelluric data were calculated using the same settings as the field data survey provided in the next section. The direct current resistivity data were observed using 41 electrodes at 10 levels (n = 1, 3, 5, 7, 9, 11, 13, 15, 17 and 19). The distance between each consecutive electrode (a) was set at 5 metres. In total, 600 apparent resistivities were obtained for left- and right-side pole-dipole (AMN and MNB) configurations. Synthetic radiomagnetotelluric data were also calculated for 25 stations at four frequencies, 234, 126, 53 and 18.3 kHz, yielding a total of 400 data for both TE- (transverse

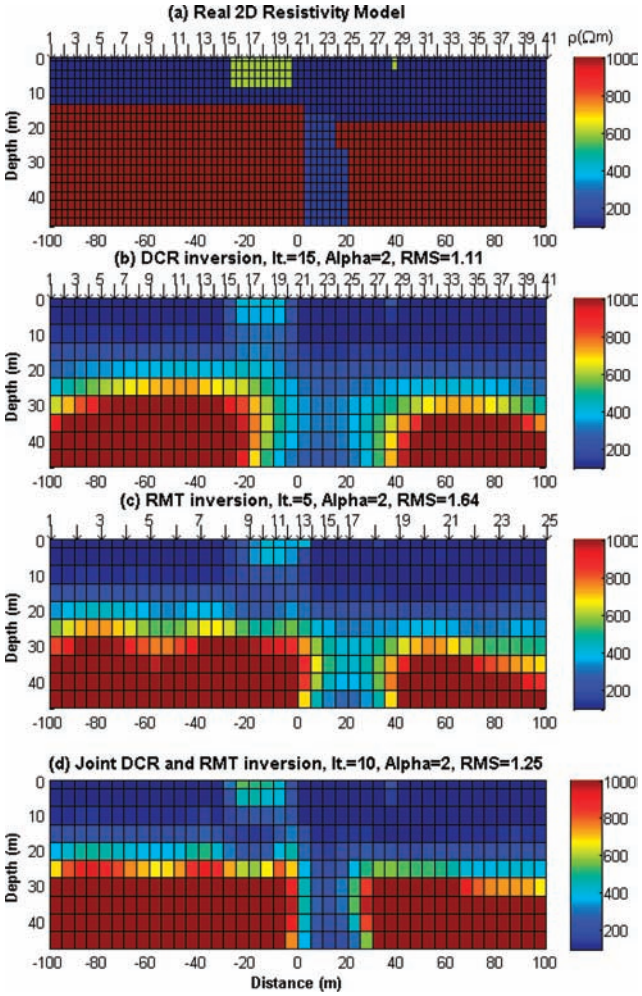

Figure 1 (a) 2D resistivity model, (b) 2D inversion result using direct current resistivity data, (c) 2D inversion result using radiomagnetotelluric data and (d) 2D joint inversion result using direct current resistivity and radiomagnetotelluric data that were calculated for the real 2D resistivity model shown in this Fig. 1(a). Electrode locations are shown on both the top of the real model and the inverted model for direct current resistivity data with a down arrow symbol. The station locations are also shown on top of the radiomagnetotelluric inverted models.

electric: where the electric field is parallel to the strike direction) and TM-modes (transverse magnetic: where the magnetic field is parallel to the strike direction), apparent resistivities and impedance phase values. The distance between each consecutive station for the first nine and last nine stations was 10 metres. The station interval was 5 metres between stations 9 and 16.

For all inversion runs, a homogenous half-space was used as a starting model with a resistivity of 195 Ωm that corresponded to the average of the apparent resistivities calculated for direct current resistivity, TE- and TM-mode apparent resistivities. Five percent Gaussian noise was added to all of the data sets before inversion and these data were used as measured data. The model mesh used in the inversion had 48 blocks in the x-direction and 13 blocks in the z-direction, yielding a total of 624 blocks. Note that most of the boundaries of the resistivity structure did not coincide with the segments of the block interface used in the model mesh during inversion (see Fig. 1). The regularization parameter, α (equation (1)), has an important influence on the 2D inversion solution. Unfortunately, there is no unique approach to selecting this parameter. The L-curve criteria and generalized cross-validation methods (Haber and Oldenburg, 2000; Hansen, 2001) can be applied to obtain this parameter. After several inversions, a value of 2 was selected for this parameter as it provided the best image in our inversion results (Figs 1b–d) for the 2D model displayed in Fig. 1(a). This value was then used with a similar approach for the field application.

The individual inversion results for direct current resistivity and radiomagnetotelluric data are shown in Figs 1(b) and 1(c). The RMS error was reduced from 4.28 to 1.11 after 15 iterations for the direct current resistivity inversion. The surface resistivity bodies could be detected. However, the layer interface and the dyke body were not acquired well. The estimated depth of the surface layer was deeper than the correct depth; in particular, the lateral extension of the dyke was overestimated. On the other hand, the RMS error was reduced from 10.77 to 1.64 after only 5 iterations for the TE- and TM-mode joint inversions of the radiomagnetotelluric data. The fault gauge body was accurately represented. However, the layer interface and the two near-surface resistive bodies could not be resolved well. The skin depth range for a 100 Ωm half-space for the radiomagnetotelluric frequencies used here is approximately between 9 and 50 metres. It is likely that this is the reason why the radiomagnetotelluric data inversion could not resolve these near-surface resistive bodies.

The joint inversion of radiomagnetotelluric with direct current resistivity is shown in Fig. 1(d). The RMS error was reduced from 7.91 to 1.25 after 10 iterations. This value lies between those obtained for the inversion of individual data sets (e.g., Sasaki 1989). As expected, the joint inversion result matches the true model more closely than either of the inversion results from individual data sets; the near-surface resistive bodies, the layer interface and the fault gauge body are well defined and there were no artefacts near the surface. During the joint inversion, the effect of radiomagnetotelluric data on the solution was decreased for the near-surface block

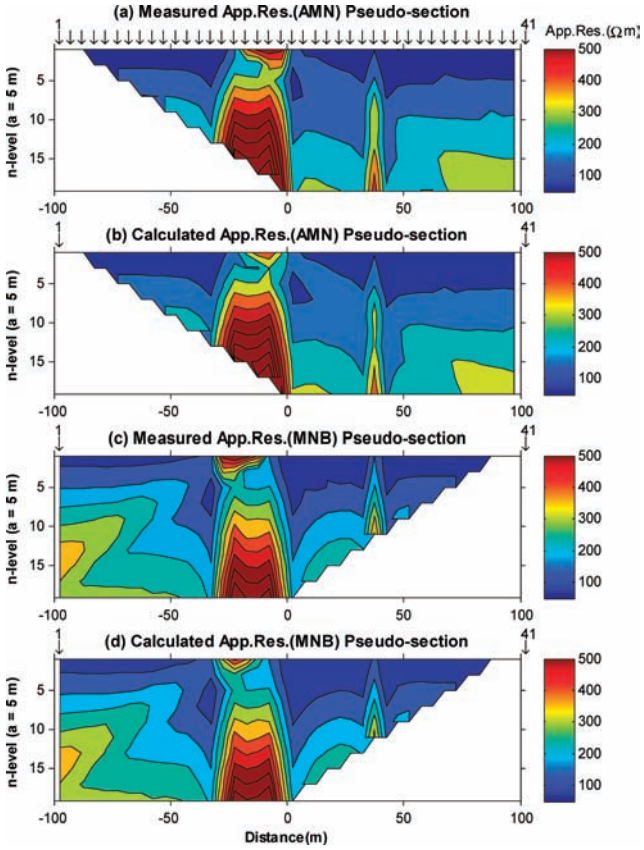

Figure 2 Measured and calculated apparent resistivity pseudo-sections for AMN (a and b) and MNB (c and d) configurations, respectively. The measured data were generated from the forward solution of the model shown in Fig. 1(a) and the calculated data obtained from the forward solution of the estimated model shown in Fig. 1(d). The electrode locations are shown in the top of the AMN apparent resistivity pseudo-sections with down arrows.

resistivity by changing the $\mathbf{W}_{\mathrm{RMT}}$ matrix element related to the near-surface blocks.

The fit between the measured (for the model in Fig. 1a) and calculated direct current resistivity data (for the estimated model shown in Fig. 1d) is shown in Fig. 2 as pseudo-sections. A good direct current resistivity data fit was obtained. The measured (for the model in Fig. 1a) and calculated (for the model in Fig. 1d) apparent resistivities and impedance phase curves both for the TE- and TM-modes are shown in Fig. 3. The fit was good for the TE mode data but poorer for the TM mode data, particularly for the stations close to the resistive bodies near the surface.

In addition, the sensitivity analysis was carried out for the models shown in Fig. 1. The model resolution matrix (e.g., Alumbaugh and Newman 2000; Friedel 2003; Stummer, Maurer and Green 2004; Özürlan *et al.* 2006; Wilkinson *et al.* 2006) was used to estimate the resolution quality of the estimated models derived from direct current resistivity, radiomagnetotelluric and the joint inversion results. The model resolution matrix is defined as (Alumbaugh and Newman 2000; Stummer *et al.* 2004):

$$R = \left(\mathbf{A}^{\mathrm{T}}\mathbf{W}_{\mathrm{d}}^{\mathrm{T}}\mathbf{W}_{\mathrm{d}}\mathbf{A} + \alpha\mathbf{C}^{\mathrm{T}}\mathbf{C}\right)^{-1}\mathbf{A}^{\mathrm{T}}\mathbf{W}_{\mathrm{d}}^{\mathrm{T}}\mathbf{W}_{\mathrm{d}}\mathbf{A} \qquad (5)$$

and its diagonal elements were displayed as 2D model sections for direct current resistivity, radiomagnetotelluric and joint direct current resistivity-radiomagnetotelluric inversion in Figs 4(a–c), respectively. The high values (blue colour) show that each of the corresponding blocks is well resolved. Approximately the first 25 m of the three estimated models (Fig. 4) yielded high resolution. However, the resistivities of blocks beneath the beginning and end of the profile are not well resolved by the direct current resistivity inversion (Fig. 4a) but are better resolved by the radiomagnetotelluric inversion (Fig. 4b). Direct current resistivity data do not have sufficient information to resolve these blocks with regards to depth of investigation (Oldenburg and Li 1999). As expected, deeper resistivities of blocks are better resolved by the radiomagnetotelluric model rather than by the direct current resistivity model. According to the magnitude of the diagonal elements of the model resolution matrix, the resistivities of both the shallower and deeper blocks are better resolved by the joint inversion of direct current resistivity and radiomagnetotelluric data (Fig. 4c) rather than by individual inversions of each corresponding data sets (Figs 4a and b). The sensitivity analysis also proved that the model resolution is improved by the joint inversion of radiomagnetotelluric and direct current resistivity data sets.

INVERSION OF FIELD DATA

The field radiomagnetotelluric and direct current resistivity data were collected in July 2003 from the Kerpen test site located south-west of the city of Kerpen, approximately 20 km west of Cologne, Germany. The geological map indicates a minor, left-stepping, suspected fault traversing the site at nearly a north-south strike (Fig. 5a). The fault is part of the Erft fault system whose main strand, the Horrem fault, passes approximately 3 km east of the site (Streich 2003). Streich (2003) gave detailed geological information regarding the area and also investigated the fault location by using different geophysical methods (direct current resistivity, seismic and georadar).

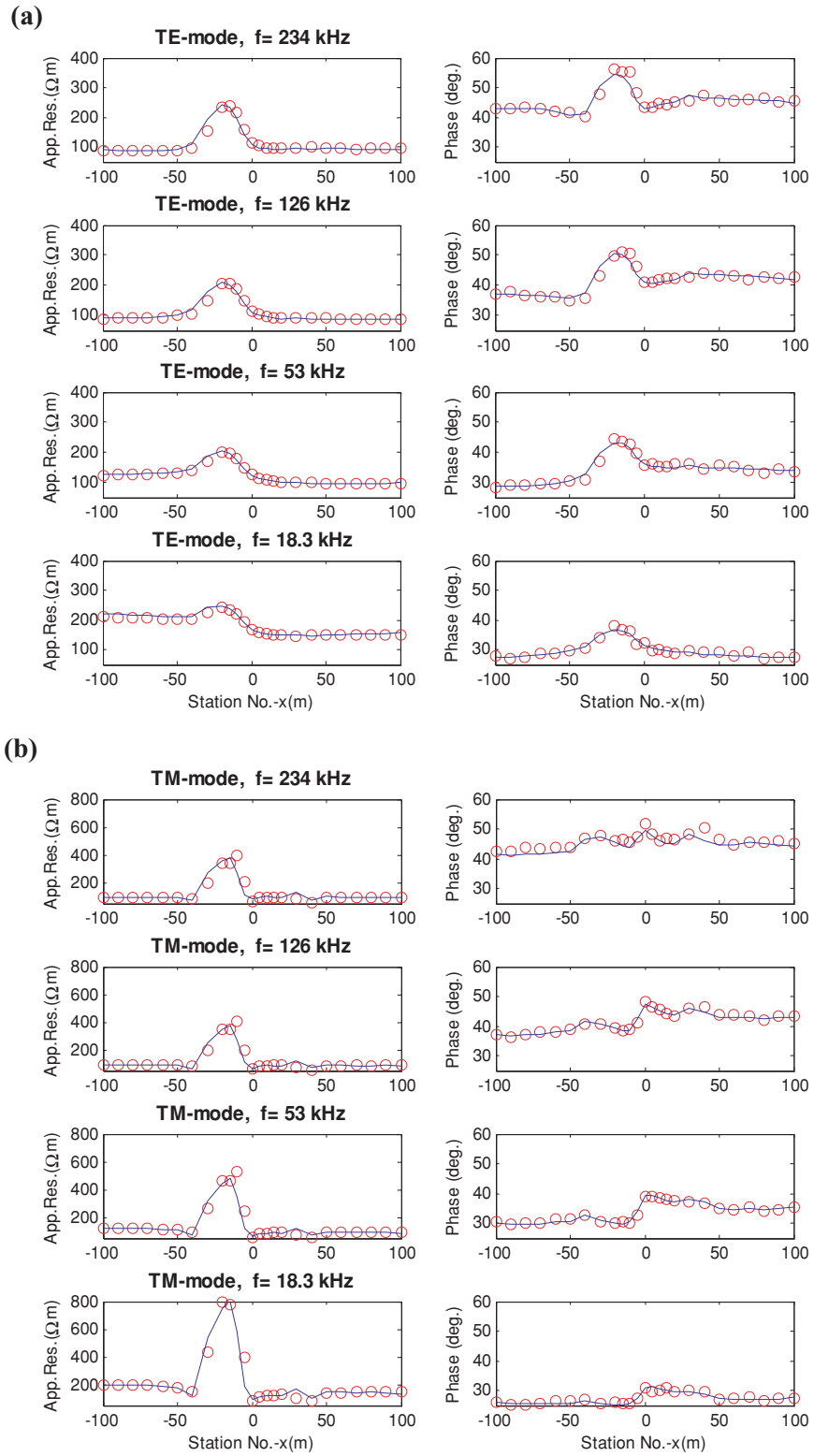

Figure 3 Comparison between measured (for the model shown in Fig. 1a) and calculated (for the estimated model shown in Fig. 1d) apparent resistivities and impedance phase data for (a) TE- and (b) TM-mode. The circular symbols represent the measured data (calculated for the real model in Fig. 1(a) and with an added noise) for four TE- and TM-mode radiomagnetotelluric frequencies. The solid lines denote the calculated data obtained from the estimated model shown in Fig. 1(d).

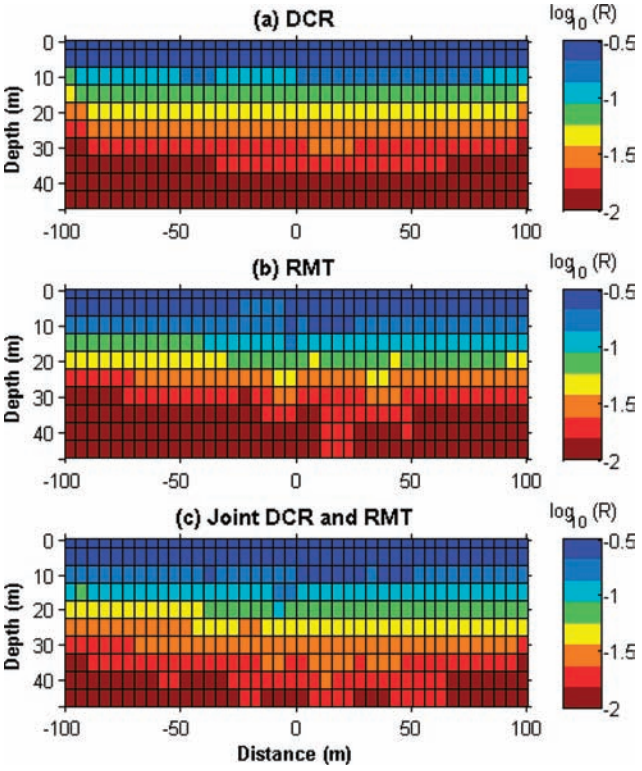

Figure 4 Diagonal elements of the resolution matrix (equation (5)) for (a) direct current resistivity, (b) radiomagnetotelluric and (c) joint direct current resistivity and radiomagnetotelluric models shown in Fig. 1.

Streich (2003) showed a 2D inversion result for the direct current resistivity data. However, due to insufficient distance between the electrodes, the 2D resistivity model only resolves the first 16 metres. The fault structure, however, is expected to be at a greater depth. According to previous geological works (e.g., Ahorner 1962; von Kamp 1986; Klostermann 1992) and the investigation of Streich (2003), the underground geology of the site consists of low-resistivity loess overlapping a high-resistivity gravel. Furthermore, the loess may be thicker in the western part of the fault. The normal fault has low resistivity, which is a typical feature of such fault zones (McCalpin 1996). The fault may only be seen in the highly-resistive gravel layer (Fig. 5a).

The purpose of this survey was the detection of the location of the fault and the resistivity structure beneath the survey area by using radiomagnetotelluric and direct current resistivity methods. A well tested radiomagnetotelluric device (Turberg and Barker 1993; Tezkan *et al.* 2000; Seher and Tezkan 2007) was used in this survey. Radio transmitters broadcasting in the frequency range between 10 kHz and 240 kHz were used and transfer functions (apparent resistivities and phases) for selected frequencies were measured in the scalar mode. Radio transmitters were chosen perpendicular and parallel to the assumed strike direction of the 2D anomaly, which can be associated to the TE and TM modes of the EM field. We collected radiomagnetotelluric data along two 200-metre long parallel lines that crossed perpendicular to the assumed strike direction of the suspected fault (Fig. 5b). The distance between the lines was approximately 115 metres. The TE- and TM-mode apparent resistivity and impedance phase values in scalar mode were collected at 25 stations, for four frequencies, 234, 183, 75 and 16.4 kHz (TE) and for three frequencies, 198, 65.8 and 12.1 kHz (TM), respectively, yielding 350 data points (apparent resistivities and impedance phases). The distance between each consecutive station was 10 m. The expected boundary of the fault was densely sampled with a station interval of 5 m. The direct current resistivity data were also collected along the same parallel lines by using an ABEM SAS 1000 imaging system with 41 electrodes with left- and right-side pole-dipole configurations. The distance between each consecutive electrode was 5 metres and the data were collected for fixed distances between the potential electrode (MN = a = 5 metres) and for 10 levels (n = 1, 3, 5, 7, 9, 11, 13, 15, 17 and 19).

The 2D inversion results, using our new algorithm with direct current resistivity and radiomagnetotelluric data collected along Line-2 (Fig. 5b), are shown in Figs 6(a) and 6(b), respectively. The direct current resistivity data inversion result was obtained after 14 iterations with a value of 1.14 for the RMS, while the radiomagnetotelluric data inversion result was obtained after 5 iterations with a RMS of 1.97. The 2D direct current resistivity inversion result shows a good conductive loess surface layer ($\rho \leq 100$ ohm - m) dropping to a depth of approximately 20 metres. Beneath this layer a relative resistive gravel layer ($\rho \geq 2000$ ohm - m) is visible and is interrupted by a conductive dyke structure ($\rho \leq 500$ ohm - m). The three layer Earth models can be derived from the radiomagnetotelluric data inversion. The fault trace can also be distinguished in the radiomagnetotelluric resistivity model but the image was not as clear as in the direct current resistivity data inversion. The joint inversion result was obtained after 8 iterations with a RMS of 1.95 (Fig. 6c). Here, we can distinguish the fault trace more accurately than in the individual inversion results by using radiomagnetotelluric and direct current resistivity data. We observe that the fault depth from the surface is approximately 16 metres. As outlined in the previous geological and geophysical study, the interface between the low-resistivity surface layer and the underlying high-resistivity layer was clearly detected.

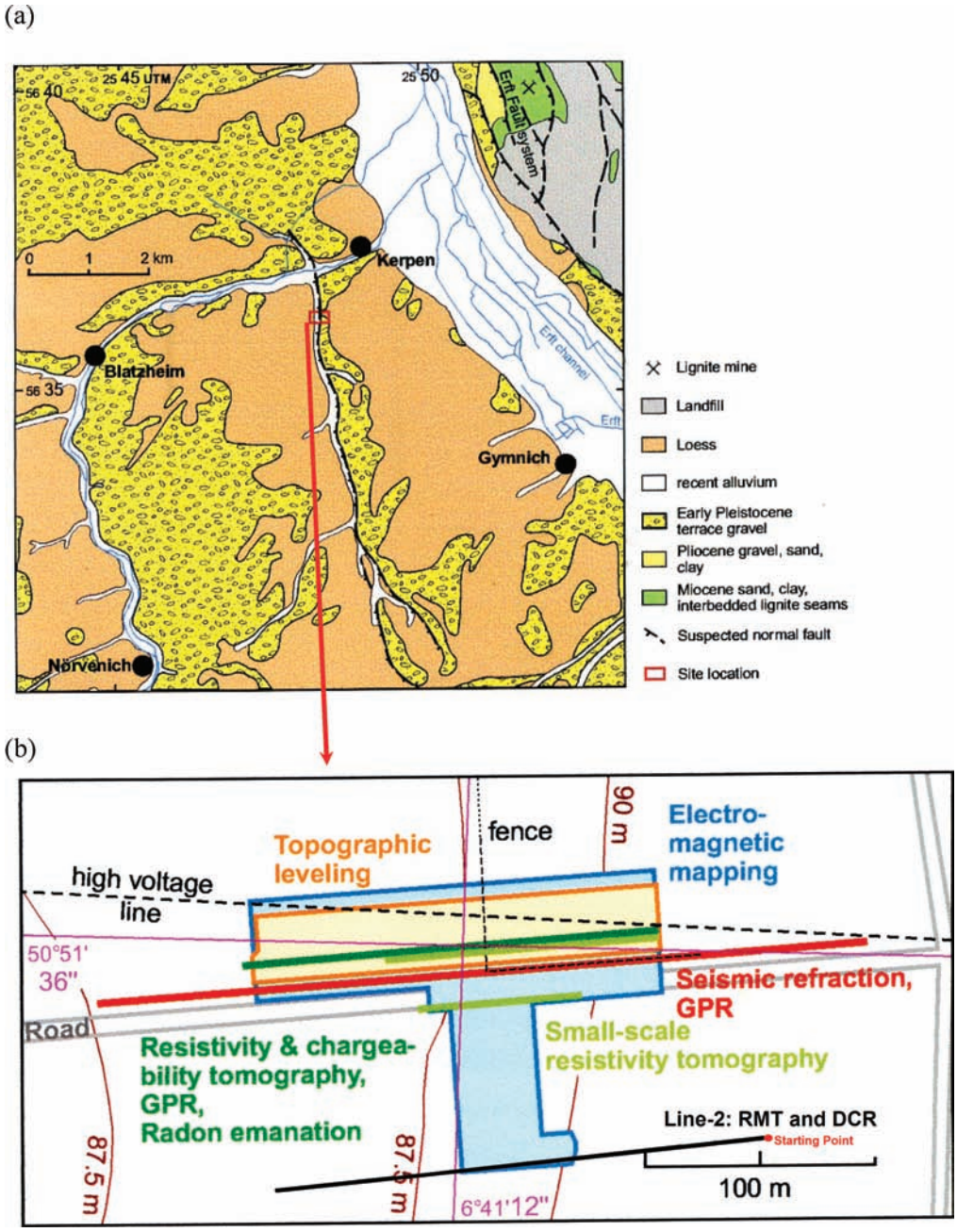

Figure 5 (a) Simplified geological map view of the vicinity of the Kerpen site (after Streich 2003). (b) Radiomagnetotelluric and direct current resistivity measurement line (Line-2) and the previous measurement locations of Streich (2003) at the Kerpen site. Line-3 is 115 metres south of Line-2. Because of the logistical difficulties, the starting point of Line-3 was moved approximately 10 metres west of the starting point of Line-2.

It can also be observed that the location of the fault was determined by the low resistivity zone inside the gravel layer. The fits between the measured and calculated direct current resistivity and radiomagnetotelluric data (for the estimated model obtained from the joint inversion in Fig. 6c) are shown in Figs 7 and 8, respectively.

We also used the model resolution matrix to estimate the resolution quality of the estimated model derived from the field data inversion. Figure 9(a–c) displays the diagonal elements of the model resolution matrix of the estimated models derived from direct current resistivity, radiomagnetotelluric and joint direct current resistivity and radiomagnetotelluric data

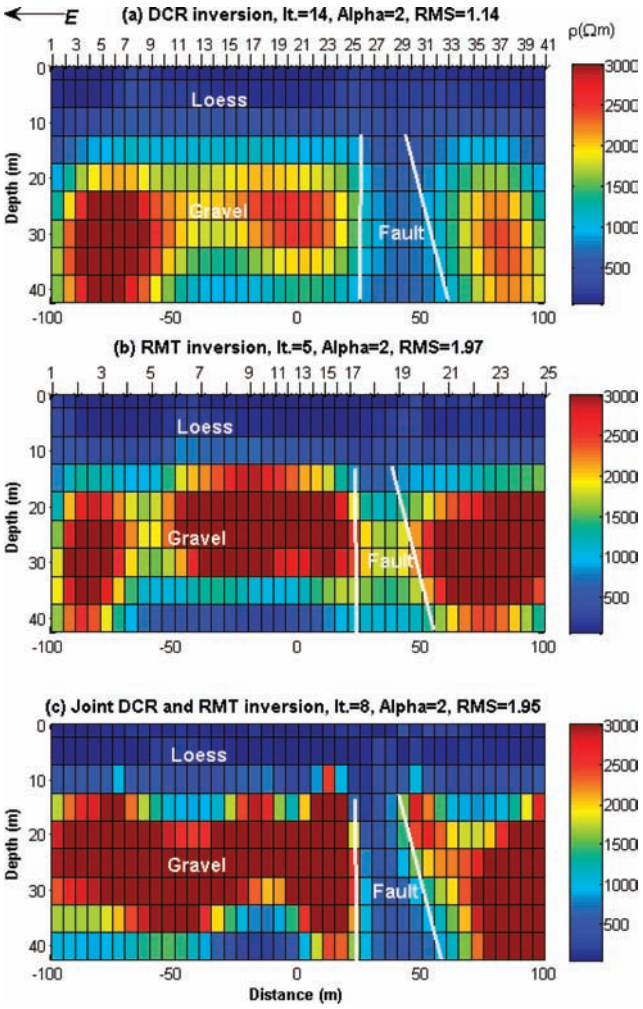

Figure 6 The estimated models obtained from the 2D inversion of (a) direct current resistivity, (b) radiomagnetotelluric and (c) joint direct current resistivity and radiomagnetotelluric data set collected along Line-2 at the Kerpen site. The electrode and station locations used to collect direct current resistivity and radiomagnetotelluric data are shown on the top of the direct current resistivity and radiomagnetotelluric inverted models, respectively, with down arrow symbols.

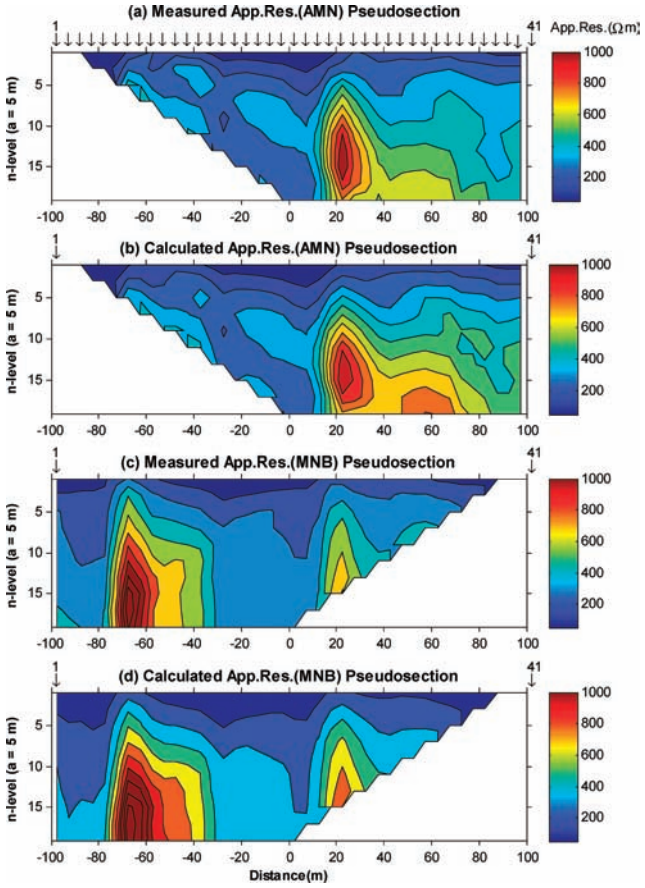

Figure 7 Measured (along Line-2, Kerpen site) and calculated apparent resistivity pseudo-sections for AMN (a and b) and MNB (c and d) configurations, respectively. Calculated apparent resistivity pseudo-sections obtained from the 2D joint inversion result (Fig. 5c).

inversion for Line-2, respectively. Similar to the synthetic data inversion, resistivities of the blocks beneath the beginning and end of the profile are not well resolved by the direct current resistivity inversion (Fig. 9a), whereas deeper blocks are better resolved by the radiomagnetotelluric model rather than by the direct current resistivity model. According to the magnitude of the diagonal elements of the model resolution matrix the resistivities of both shallower and deeper blocks are better resolved by the joint inversion of direct current resistivity and radiomagnetotelluric data (Fig. 9c) rather than by individual inversions of each corresponding data sets.

We inverted the radiomagnetotelluric and direct current resistivity data collected along Line-3 shown in Figs 10(a) and 10(b). This line is parallel to Line-2 and approximately 115 south of it. The joint inversion result is given in Fig. 10(c). The number of iterations and RMS values are shown in the top part of each corresponding model. The inversion results show a similar resistivity structure as was obtained from the inversion of the data sets collected along Line-2. However, the fault location is found approximately 10 metres east of the fault location found along Line-2. The starting points of Line-2 and Line-3 were not the same. The starting point of Line-3 was moved 10 metres west of Line-2 for logistical reasons. This may explain why the fault location was not found at the same location in both of the estimated models.

Again, we can see that the fault is better distinguished in the joint inversion result (see Fig. 10c). The observed and the

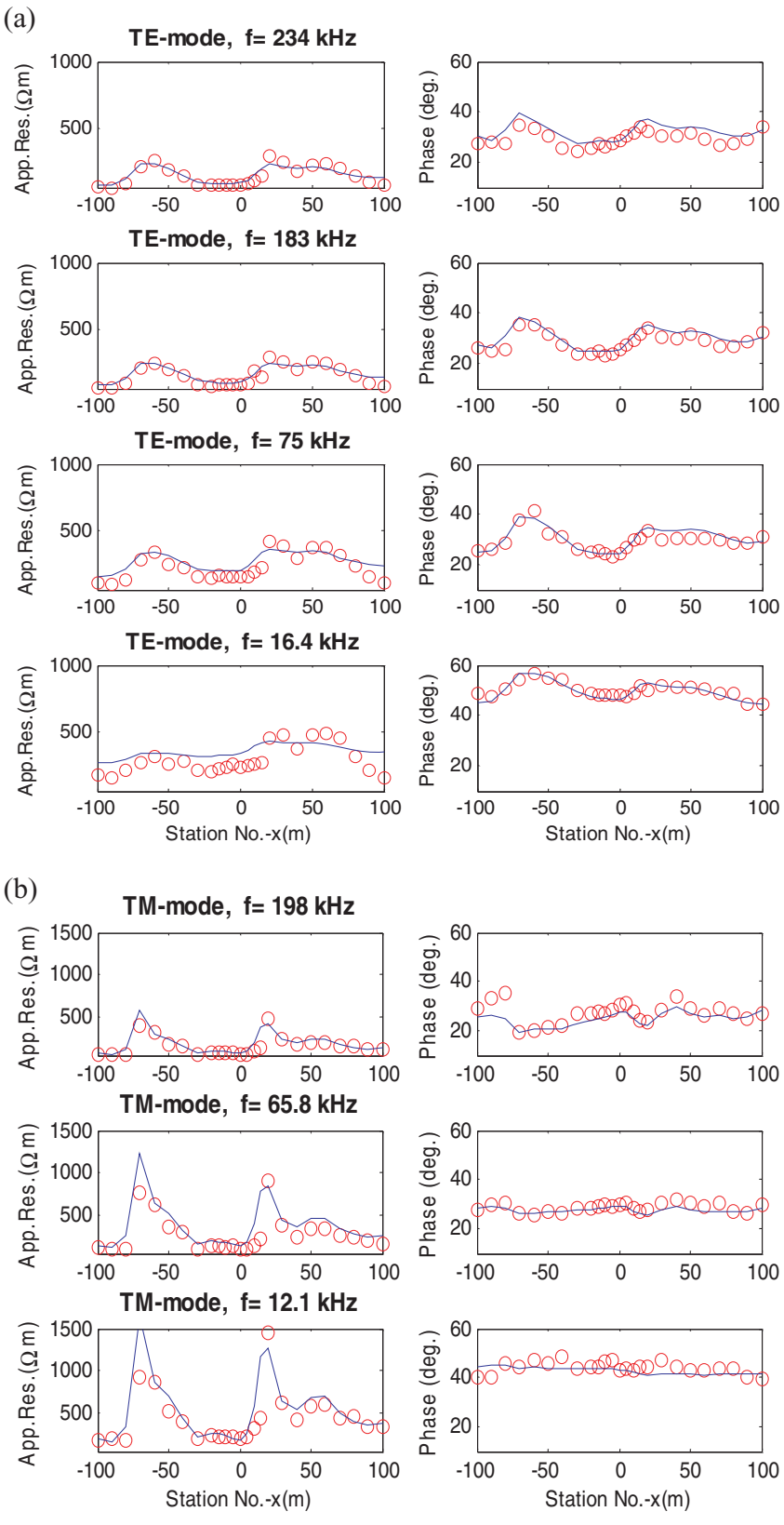

Figure 8 Comparison between measured data collected along Line-2 and calculated data obtained from the estimated model shown in Fig. 5(c), for (a) TE- and (b) TM-mode.

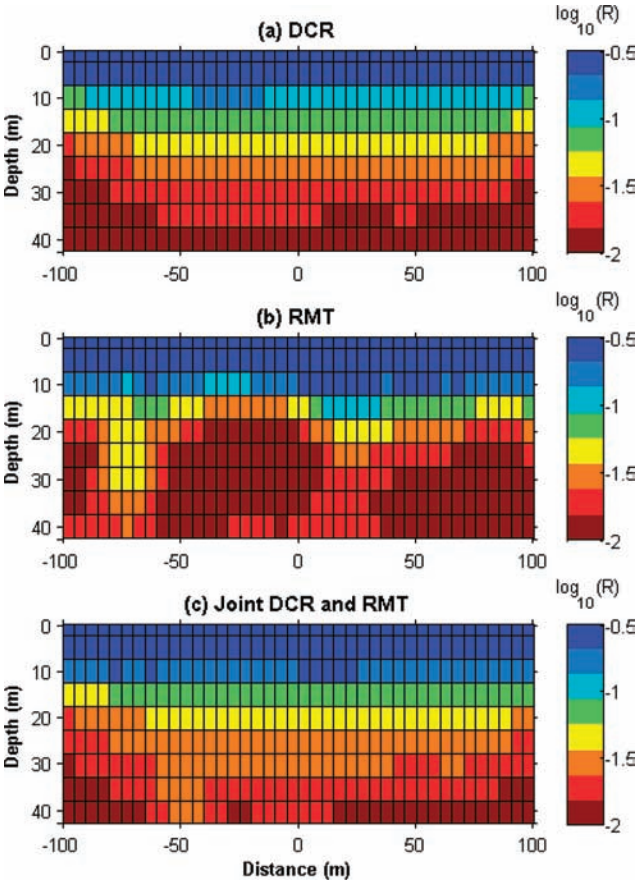

Figure 9 Diagonal elements of the resolution matrix (equation (5)) for (a) direct current resistivity, (b) radiomagnetotelluric and (c) joint direct current resistivity and radiomagnetotelluric models shown in Fig. 6.

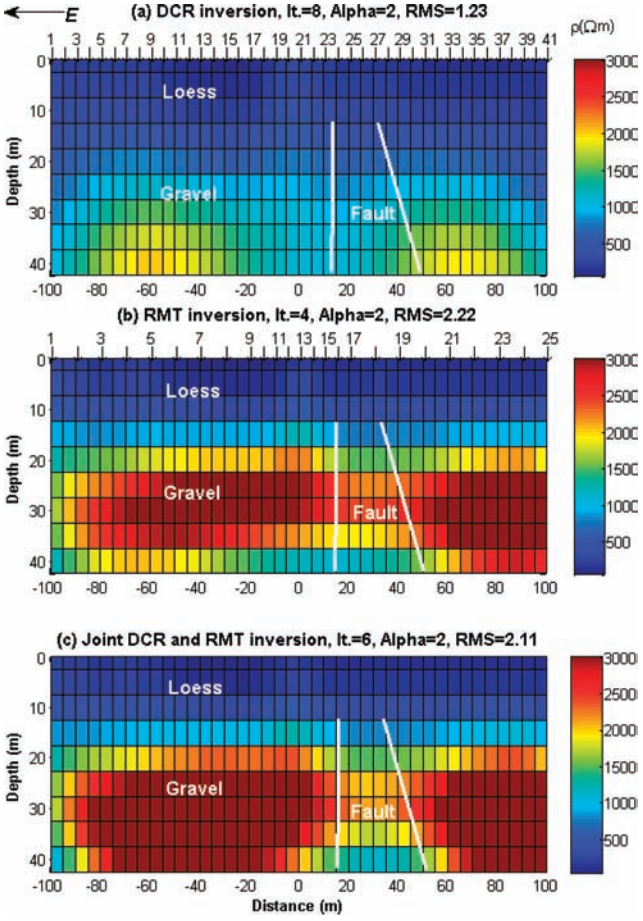

Figure 10 The estimated models obtained from 2D inversion of (a) direct current resistivity, (b) radiomagnetotelluric and (c) joint direct current resistivity and radiomagnetotelluric data set collected along Line-3 at the Kerpen site.

calculated data fit can also be acknowledged and diagonal elements of the model resolution matrix also showed that the joint inversion improved the resolving power of block resistivities. The joint inversion of the field radiomagnetotelluric and direct current resistivity measurements illustrates that the direct current resistivity data have provided complementary information for the inversion of radiomagnetotelluric data and vice versa.

CONCLUSIONS

We have developed a new 2D joint inversion algorithm for radiomagnetotelluric and direct current resistivity data. Synthetic data inversion results showed that small-scale near-surface bodies cannot be acquired from radiomagnetotelluric inversion results. However, radiomagnetotelluric data can be affected by small-scale near-surface bodies, which can cause a static shift effect and radiomagnetotelluric inversions sometimes generate blurred images due to this effect and the non-uniqueness of the radiomagnetotelluric inversion problem. On the other hand, the direct current resistivity method can resolve these near-surface blocks. We inverted the direct current resistivity and radiomagnetotelluric data jointly and resolved both near-surface and deeper structures. The joint inversion of radiomagnetotelluric and direct current resistivity measurements provided here reduces the non-uniqueness and improves the model resolution and quality of the interpretation.

Field radiomagnetotelluric and direct current resistivity data were collected at the Kerpen test site. Comparison of the individual and joint inversions of the radiomagnetotelluric and direct current resistivity measurements showed that the best joint inversion can recover the underground resistivity structure. The results of the field data inversion indicated the nor-

mal fault location to be approximately 16 metres below the surface.

ACKNOWLEDGEMENTS

This work was supported by TÜBİTAK under Project No. 104Y073 and was performed in the Geoscience Data Processing Laboratory (YEBVIL) at Ankara University, Turkey. M.E. Candansayar was granted postdoctoral fellowships by TÜBİTAK (Scientific and Technical Research Council of Turkey) and DFG (Deutsche Forschungsgemeinschaft) in 2005. We thank R. Berges for his assistance in the field survey.

REFERENCES

Ahorner L. 1962. Untersuchungen zur quartären Bruchteknoik der Niederrheinischen Bucht. *Eiszeitalter und Gegenwart* **13**, 24–105.

Alumbaugh D. and Newman G. 2000. Image appraisal for 2-D and 3-D electromagnetic inversion. *Geophysics* **65**, 1455–1467.

Auken E., Pellerin L., Christensen N.B. and Sørensen K. 2006. A survey of current trends in near-surface electrical and electromagnetic methods. *Geophysics* **71**, G249–G260.

Candansayar M.E. 2006. Combined two-dimensional inversion of four- and three-electrode arrays resistivity data. Near Surface 2006, Helsinki, Finland, Expanded Abstracts.

Candansayar M.E. 2008. Two-dimensional inversion of magnetotelluric data with consecutive use of conjugate gradient and least-squares solution with singular value decomposition algorithms. *Geophysical Prospecting* **56**, 141–157.

Candansayar M.E. and Basokur A.T. 2001. Detecting small-scale targets by the 2D inversion of two-sided three-electrode data: Application to an archaeological survey. *Geophysical Prospecting* **49**, 13–25.

Candansayar M.E. and Tezkan B. 2006. A comparison of different radiomagnetotelluric data inversion methods for buried waste sites. *Journal of Applied Geophysics* **58**, 218–231.

Dey A. and Morrison H.F. 1978. Resistivity modelling for arbitrarily shaped two-dimensional structures. *Geophysical Prospecting* **27**, 106–136.

Friedel S. 2003. Resolution, stability and efficiency of resistivity tomography estimated from a generalized inverse approach. *Geophysical Journal International* **153**, 305–316.

Gallardo L.A. and Meju M.A. 2004. Joint two-dimensional dc resistivity and seismic travel-time inversion with cross-gradients constraints. *Journal of Geophysical Research* **109**, B03311. doi:10.1029/2003JB0022717.

Haber E. and Oldenburg D. 2000. A GCV Bases method for non-linear ill-posed problems. *Computational Geosciences* **4**, 41–63.

Hansen P.C. 2001. Regularization Tools: A MATLAB package for analysis and solution of discrete ill-posed problems. Report, Technical University of Denmark, Denmark (downloaded from http://www.imm.dtu.dk/~pch).

Harinarayana T. 1999. Combination of EM and DC measurement for upper crustal studies. *Surveys in Geophysics* **20**, 257–278.

von Kamp H. 1986. *Geologische Karte von Nordrhein-Westfalen 1:100000, Blatt C5106 Köln*. Geological Survey of Northrhine-Westphalia, Krefeld, Germany.

Klostermann J. 1992. *Das Quartär der Niederrheinischen Bucht: Ablagerungen der letzten Eiszeit am Niederrhein*. Geological Survey of Northrhine-Westphalia, Krefeld.

Linde N. and Pedersen L.B. 2004. Characterization of a fractured granite using radio magnetotelluric (RMT) data. *Geophysics* **69**, 1155–1165.

McCalpin J.P. 1996. *Paleoseismology*. Academic Press. ISBN 0124818269

McGillivray P.R., Oldenburg D.W., Ellis R.G. and Habashy T.M. 1994. Calculation of sensitivities for the frequency-domain electromagnetic problem. *Geophysical Journal International* **116**, 1–4.

McNeill J.D. and Labson V. 1991. Geological mapping using VLF radio fields. In: *Electromagnetic Methods in Applied Geophysics* (ed.M.N. Nabighan), pp. 521–640. Society of Exploration Geophysicists. ISBN 1560800224

Meju M. 1996. Joint inversion of TEM and distorted MT soundings: Some effective practical considerations. *Geophysics* **61**, 56–65.

Newman G., Recher S., Tezkan B. and Neubauer F.M. 2003. Three-dimensional inversion of a radiomagnetotelluric field data set. *Geophysics* **68**, 791–802.

Oldenburg D.W. and Li Y. 1999. Estimating depth of investigation in DC resistivity and IP surveys. *Geophysics* **64**, 403–416.

Özürlan G., Candansayar M.E. and Şahin H.M. 2006. Deep resistivity structure of Dikili- Bergama region, West Anatolia, revealed by two dimensional inversion of vertical electrical sounding data. *Geophysical Prospecting* **54**, 187–197.

Pedersen L.P., Bastani M. and Dynesius L. 2005. Groundwater exploration using combined controlled-source and radiomagnetotelluric techniques. *Geophysics* **70**, G8–G15.

Raiche A.P., Jupp D.L.B., Rutter H. and Vozoff K. 1985. The joint use of coincident loop transient electromagnetic and Schlumberger sounding to resolve layered structures. *Geophysics* **50**, 1618–1627.

Sasaki Y. 1989. Two-dimensional joint inversion of MT and dipole-dipole resistivity data. *Geophysics* **54**, 254–262.

Seher T. and Tezkan B. 2007. Radiomagnetotelluric and direct current resistivity measurements for the characterization of conducting soils. *Journal of Applied Geophysics* **63**, 35–45.

Smith N.C. and Vozoff K. 1984. Two-dimensional DC resistivity inversion for dipole-dipole data. *IEEE Transactions on Geoscience and Remote Sensing* **22**, 21–28.

Streich R. 2003. *Geophysical prospecting of suspected Holocene fault activity in the Lower Rhine Embayment, Germany*. PhD thesis, Potsdam University, Germany.

Stummer P., Maurer H. and Green A.G. 2004. Experimental design: Electrical resistivity data sets that provide optimum subsurface information. *Geophysics* **69**, 120–139.

Tezkan B. 1999. A review of environmental application of quasi stationary electromagnetic techniques. *Survey in Geophysics* **20**, 279–308.

Tezkan B., Goldman M., Greinwald S., Hördt A., Müller I., Neubauer F.M. and Zacher G. 1996. A joint application of

radiomagnetotellurics and transient electromagnetics to the investigation of a waste deposit in Cologne (Germany). *Journal of Applied Geophysics* **34**, 199–212.

Tezkan B., Hördt A. and Gobashy M. 2000. Two dimensional radiomagnetotelluric investigations of industrial and domestic waste sites in Germany. *Journal of Applied Geophysics* **44**, 237–256.

Tikhonov A.N., Goncharsky A.V., Stepanov V.V. and Yagola A.G. 1995. *Numerical Methods for the Solution of Ill-posed Problems*. Kluwer Academic Publishers. ISBN 079233583X.

Tripp A.C., Hohmann G.W. and Swift C.M. 1984. Two-dimensional resistivity inversion. *Geophysics* **49**, 1708–1717.

Turberg P. and Barker R. 1996. Joint application of radiomagnetotelluric and electrical imaging surveys in complex surface environments. *First Break* **14**, 105–112.

Wilkinson P.B., Meldrum P.I., Chambers J.E., Kuras O. and Ogilvy R.D. 2006. Improved strategies for the automatic selection of optimised sets of electrical resistivity tomography measurement configurations. *Geophysical Journal International* **167**, 1119–1126.

Vozoff K. and Jupp D.L.B. 1975. Joint inversion of geophysical data. *Geophysical Journal of the Royal Astronomical Society* **42**, 977–991.